



저작자표시-비영리-변경금지 2.0 대한민국

이용자는 아래의 조건을 따르는 경우에 한하여 자유롭게

- 이 저작물을 복제, 배포, 전송, 전시, 공연 및 방송할 수 있습니다.

다음과 같은 조건을 따라야 합니다:



저작자표시. 귀하는 원저작자를 표시하여야 합니다.



비영리. 귀하는 이 저작물을 영리 목적으로 이용할 수 없습니다.



변경금지. 귀하는 이 저작물을 개작, 변형 또는 가공할 수 없습니다.

- 귀하는, 이 저작물의 재이용이나 배포의 경우, 이 저작물에 적용된 이용허락조건을 명확하게 나타내어야 합니다.
- 저작권자로부터 별도의 허가를 받으면 이러한 조건들은 적용되지 않습니다.

저작권법에 따른 이용자의 권리는 위의 내용에 의하여 영향을 받지 않습니다.

이것은 [이용허락규약\(Legal Code\)](#)을 이해하기 쉽게 요약한 것입니다.

[Disclaimer](#)

공학석사 학위논문

Magnetic Actuation of Auxetic
Chiral Stents Composed of
Magnetic Nanoparticles–polymer
composites

자성나노입자-폴리머 복합체로 이루어진 스텐트의
동작 제어 연구

2023년 2월

서울대학교 대학원

공과대학 재료공학부

오연주

Magnetic Actuation of Auxetic Chiral Stents Composed of Magnetic Nanoparticles–polymer composites

지도 교수 유 응 열

이 논문을 공학석사 학위논문으로 제출함
2023년 2월

서울대학교 대학원
공과대학 재료공학부
오 연 주

오연주의 공학석사 학위논문을 인준함
2023년 2월

위 원 장	<u> 안 철 희 </u>	(인)
부위원장	<u> 유 응 열 </u>	(인)
위 원	<u> 박 찬 </u>	(인)

Abstract

Coronary artery disease is one of the leading causes of death worldwide. The development of bare metal stents (BMS) has been a major advance over balloon angioplasty in the management of symptomatic coronary artery disease. However, the BMS is associated with an increased risk of in-stent restenosis, very late stent thrombosis, revascularization, myocardial infarction, and death.

To overcome these clinical complications and improve patency, three-dimensional (3D)-printed auxetic anti-trichiral tubular structure and magnetic elements composed of ferrite-nanoparticle-polymer composites were fabricated. We set up the magnetic anisotropy of each magnetic element composed of magnetic particles in a polymer matrix by applying magnetic fields. The magnetic particles were arranged in chains which axis is built in the field direction. We then determined a specific arrangement of the 3D-printed auxetic anti-trichiral tubular structure for stent operation. The 3D structured stent exhibits immediate and repeatable contraction and expansion behaviors by applying static fields of 250 mT along the axial direction of its tubular structure. Furthermore, we derived an analytical model to compare the rotation angle of the individual magnet elements with the experimental results. The

analytical calculations were in good agreement with the experimentally observed actuations. Therefore, our results suggest that a magnetic field-driven actuation of specially structured stents composed of the magnetic-nanoparticle-polymer composite may be implemented to overcome the limitations of balloon angioplasty and thermally actuated polymer stents and provide an alternative way of actuation to self-expanding polymer stents.

Keyword : Self-expandable polymer stent, magnetic actuation, chiral honeycomb structures, anti-trichiral honeycomb structure, auxetic tubular structures

Student Number : 2020-22555

Table of Contents

Abstract.....	i
Table of Contents.....	iii
List of Figures.....	iv
List of Tables.....	vi
Chapter 1. Introduction.....	1
1.1. Motivation.....	1
1.2. Research Aims and Approach.....	2
Chapter 2. Research Background.....	3
2.1. Development of Coronary Artery Stents.....	3
2.2. Existing Self-expandable polymer stents.....	5
2.3. Magnetic Actuation.....	6
2.4. Chiral Honeycomb Structures.....	8
Chapter 3. Design and Modeling.....	1 1
3.1. Design Principle.....	1 1
3.2. Modeling.....	1 6
Chapter 4. Sample Fabrication.....	2 3
4.1. Fabrication Method.....	2 3
4.1.1 3D Printing of anti-trichiral honeycomb structure.....	2 4
4.1.2 Alignment Mold.....	2 6
4.1.3 Material Preparation.....	2 8
4.1.4 Alignment.....	2 9
4.1.5 Assembly.....	3 1
Chapter 5. Results.....	3 3
5.1. Magnetic Properties and Characterization.....	3 3
5.1.1 Optical Microscopy.....	3 3
5.1.2 Vibrating sample magnetometer.....	3 4
5.2. Magnetic actuation of 2D anti-trichiral honeycomb structure.....	3 6
5.3. Optimization of parameters for stent design.....	3 9
5.4. Optimization of 3D stent.....	4 5
5.4.1 Contraction according to stent thickness.....	4 5
5.4.2 Contraction according to ligament length.....	4 9
5.4.3 Optimized 3D stent prototype.....	5 2
Chapter 6. Conclusion.....	5 5
References.....	5 6
Abstract in Korean.....	5 9

List of Figures

Figure 1 (a) Planar and (b) tubular auxetic structure.....	9
Figure 2 Various types of chiral honeycomb structures.....	1 0
Figure 3 (a) Unit cell of anti-trichiral honeycomb structure (b) compressed state.....	1 3
Figure 4 Illustration of an anti-trichiral honeycomb unit cell with magnetic nanoparticle-polymer composites, actuated under magnetic fields.....	1 4
Figure 5 Concept of a magnetically actuated stent	1 5
Figure 6 Illustration of Zeeman Energy	2 0
Figure 7 Magnetic moments of dipolar interaction energy and Zeeman energy.....	2 0
Figure 8 Torque of magnetic moment and elastic energy	2 1
Figure 9 Theoretical calculation of chain angle rotation according to magnetic field.....	2 2
Figure 10 a) Unit cell and (b) tubular design of anti-trichiral honeycomb structure	2 5
Figure 11 Alignment mold for magnetic nanoparticle-polymer composites.	2 7
Figure 12 Illustration of the fabrication process of magnetic nanoparticle-polymer composites	3 0
Figure 13 Attachment of the magnetic nanoparticle-polymer composites	3 2
Figure 14 (a) Schematic of the magnetic nanoparticle-polymer composite. Arrows indicate the parallel and perpendicular direction. (b) Optical microscopic image and (c) hysteresis curves measured by VSM.	3 5
Figure 15 (a) Images of the 2D prototype under various magnetic fields. (b) Chain rotation angle under various magnetic fields. 3 7	
Figure 16 Comparison of the theoretical modeling and experimental values.	3 8
Figure 17 Illustration of major parameters of anti-trichiral honeycomb structure.....	4 1
Figure 18 Theoretical calculation results with (a) with different stent thickness, and (b) different ligament length.....	4 2
Figure 19 Experimental results of stents (a) with different stent thickness, and (b) different ligament length.....	4 3
Figure 20 Comparison of theoretical and experimental results of stents (a) with different stent thickness, and (b) different ligament length.....	4 4
Figure 21 Experimental results for 3D stent chain angle rotation with	

different stent thickness.....	4 7
Figure 22 Contraction rate of samples with different stent thickness, (a) length in the axis direction and (b) diameter.	4 8
Figure 23 Experimental results for 3D stent chain angle rotation with different ligament length.	5 0
Figure 24 Contraction rate of samples with different ligament lengths (a) length in the axis direction and (b) diameter.	5 1
Figure 25 (a) Images of the contracting anti-trichiral stent composed of magnetic nanoparticle-polymer composites and (b) chain rotation angle under various magnetic fields.....	5 3
Figure 26 Contraction rate of (a) length in the axis direction and (b) diameter.....	5 4

List of Tables

Table 1 Dimensions of the alignment mold	2 7
Table 2 Table 2. Values of the stent parameters.....	4 1

Chapter 1. Introduction

Chapter 1 introduces the overall research by explaining the motivation, research concept, and approaches. An organization of the thesis is also included for convenience.

1.1. Motivation

A stent is a metal or plastic tube inserted into the artery to relieve blockages or treat narrow or weakened arteries. As the prevalence of cardiovascular diseases increase constantly, the market size of coronary stents is also increasing. Implantation of bare-metal stents and drug-eluting stents are the most frequently performed therapy for cardiovascular diseases such as stroke or heart attack. However, due to the ongoing risk of thrombosis, in-stent restenosis, and limitations of balloon angioplasty, bioresorbable scaffolds made of biodegradable polymer and new methods for inserting stents have been developed to correspond to the growing market size. Self-expandable polymer stents have been studied using shape memory polymer activated by external stimuli, such as light or heat. Here in this study, to implement a self-expandable and easily removable stent, self-expandable polymer stents actuated by

magnetic field has been studied.

1.2. Research Aims and Approach

In the present study, to facilitate magnetic actuation, we fabricated a magnetically actuating stent by attaching magnetic nanoparticle–polymer composites to a 3D printed auxetic anti-trichiral tubular structure. By aligning the Fe_3O_4 magnetic nanoparticles within the elastomer matrix under uniform magnetic fields, the composites were programmed to have magnetic anisotropy along the chain axis. We demonstrate the 3D shape deformation of an auxetic anti-trichiral tubular structure through the rotation of composites and bending of ligaments under magnetic fields. Such magnetic actuation of the structure may offer a novel step toward developing flexible self-expandable polymer stents for coronary stents.

Chapter 2. Research Background

Chapter 2 provides background information and overview of the coronary artery stent history, existing self-expandable polymer stents, magnetic actuation of magnetic materials, and chiral honeycomb structures.

2.1. Development of Coronary Artery Stents

Due to the high prevalence of cardiovascular diseases such as stroke and heart attack, the demand for coronary stents has been growing over the decades. A stent for coronary is a metal or plastic tube inserted into the lumen of an anatomic vessel or duct to relieve blockages or treat narrow or weakened arteries. Coronary artery stents were developed to overcome the limitations of plain balloon angioplasty. The most common use for coronary stents is the coronary arteries, into which a bare-metal stent, a drug-eluting stent, a bioabsorbable stent, and bioresorbable vascular scaffolds [1]. Coronary intervention with the implantation of drug-eluting or bare-metal stents has become one of the most frequently performed therapeutic procedures in medicine [2]. The use of drug-eluting stents has been shown to be more effective in the prevention of

restenosis than the use of bare-metal stents [2]. However, a new complication has been accompanied by in-stent restenosis arising from neointimal hyperplasia. In-stent restenosis after coronary angioplasty is one of the main limitations of this procedure, leading to the recurrence of neointimal proliferation and repeat revascularization. Drug-eluting stents provide a site-specific, controlled release of antiproliferative agents targeting the suppression of neointimal hyperplasia [2]. However, drug-eluting stents are also associated with an ongoing risk of stent-related adverse events such as thrombosis, myocardial infarction, and restenosis after 1 year [2]. To prevent restenosis and eliminate long-term risks related to bare-metal stents and drug-eluting stents, bioresorbable scaffolds have been developed to provide drug delivery and mechanical support functions using naturally occurring and synthetic biodegradable polymers [3].

2.2. Existing Self-expandable polymer stents

To prevent thrombosis and in-stent restenosis, new platforms for self-expandable polymer stents have been developed to improve biodegradability and rapid expansion, minimize invasive surgery, and avoid limitations of balloon angioplasty. Most research on self-expandable polymer stents focused on shape memory polymers to activate the rapid expansion by an external stimulus, especially thermal actuation [4]. The stents for thermal actuation are temporarily locked into a thinner shape and expanded above a certain temperature depending on the material properties. Although these stents are simply fabricated and have a high recovery rate, they have a limitation of being sensitive to temperature and having biocompatibility issues, such as tissue damage on the tissues surrounding the stents upon the application of thermal stimulus [5].

2.3. Magnetic Actuation

Remote actuation of stimuli-responsive soft materials driven by external stimuli, such as heat [6], light [7, 8], solvent [9], or magnetic fields [5, 10–13] has led to the development of biomedical applications [14]. Among the various types of external stimuli, magnetically responsive soft materials have been receiving much attention in recent years due to a safe and effective remote actuation method, especially for biomedical applications.

Magnetic actuation using magnetic fields is biologically friendly and minimizes tissue damage, providing rapid, effective remote control insensitive to temperature. To improve fast contraction and expansion rate, magnetic-responsive materials such as magnetorheological elastomers (MREs) can be used for fast response to magnetic fields [15]. These magnetic nanoparticles (MNP) can be programmed in the elastomers to have magnetic anisotropy by application of an external magnetic field, where the particles assemble into chains in the direction of the applied field [16]. Moreover, magnetic actuation of polymer stents has the advantage of rapid actuation and insensitivity to temperature. The removal of stents will be easy and safe, minimizing the long-term risks of

conventional stents, such as very late stent thrombosis, myocardial infarction, in-stent restenosis, and death.

2.4. Chiral Honeycomb Structures

Materials that exhibit a negative Poisson's ratio (NPR) refer to having the cross-sections expanding (contracting) when stretched (compressed) (Figure 1) [17]. As the re-entrant honeycomb structure was found to produce the NPR effect in the 1980s [18], different types of NPR structures were proposed. Structures using rods, springs, and hinges, and special foams were designed.

Among the various NPR honeycomb structures, the chiral honeycomb structures are widely studied owing to the novel deformation mechanism exhibiting good NPR effect, and simple designability. The chiral honeycomb structure consists of rounded nodes and ligaments connecting the nodes together. The number and the position of the ligament determines the name of the structure (Figure 2) [19]. For instance, structures with three ligaments surrounding the node will be named trichiral honeycomb structure, four ligaments: tetrachiral honeycomb structure, six ligaments: hexachiral honeycomb structure, and ligaments that are connected to the same side of the nodes will be called anti-chiral honeycomb structures [20]. When the chiral honeycomb structure is stressed, the rounded node rotates, inducing the connecting ligaments to bend [21]. This unique deformation mechanism brings about the NPR

effect, which we selected to demonstrate the rotation through magnetic composites.

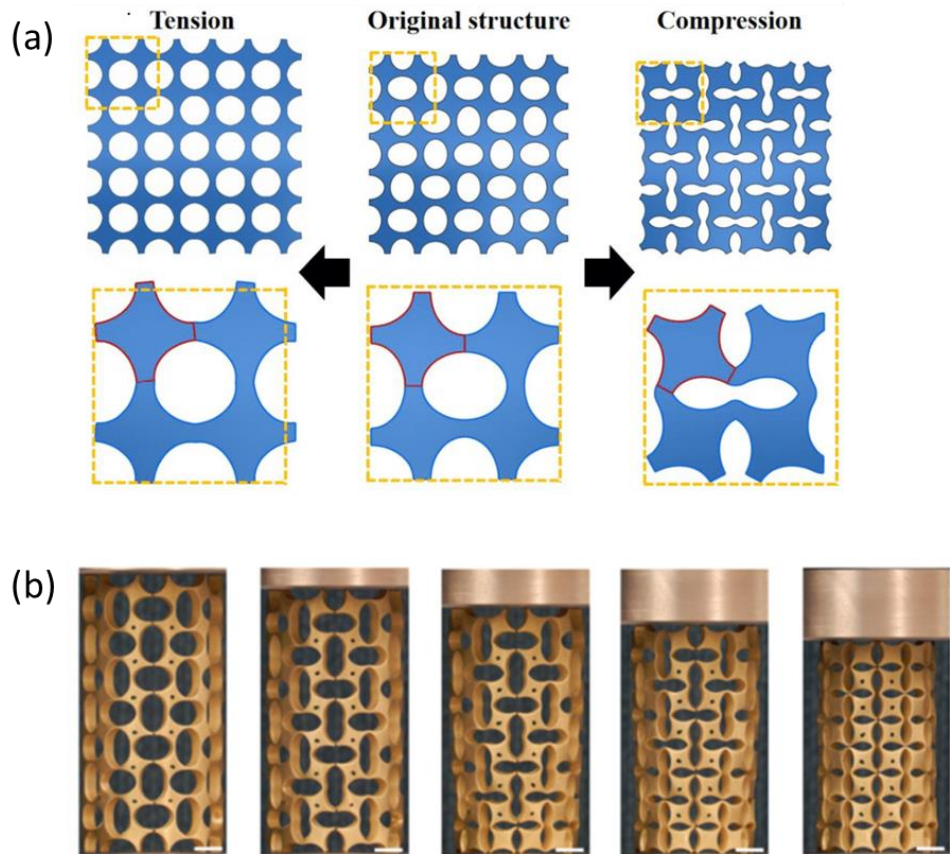


Figure 1 (a) Planar and (b) tubular auxetic structure

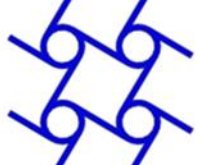
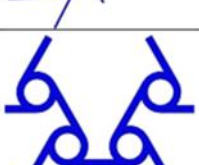
Tri-chiral		
Tetra-chiral		
Hexa-chiral		
Tri-anti-chiral		
Tetra-anti-chiral		

Figure 2 Various types of chiral honeycomb structures

Chapter 3. Design and Modeling

3.1. Design Principle

In this study, we used the anti-trichiral honeycomb structure for the magnetic stent model. The design of the anti-trichiral honeycomb structure consists of rounded nodes and ligaments connecting the nodes together. Nodes are connected by three ligaments sharing the same side, where Figure 3(a) shows the unit cell of the structure, and the compressed state in Figure 3(b).

The magnetic nanoparticle-polymer composites are attached to the empty sites of the rounded nodes, inducing the rotation of nodes under the magnetic field as illustrated in Figure 4. The deformation of the anti-trichiral honeycomb structure depends on the magnetic composites that move independently. The magnetic nanoparticles are programmed under a uniform magnetic field to have magnetic anisotropy. The morphology of the actuated anti-trichiral honeycomb shape can be controlled by the direction of the aligned MNP chains or the angle according to the actuating magnetic field. The 3D printed ligaments connect the composites together, also maintaining the overall shape. When the actuating magnetic field is applied, the rotating composites causes the ligaments to bend.

Here, the designs of the anti-trichiral tubular structure consists of 9 nodes in the axis direction and 6 nodes in the circumferential direction that are joined together by ligaments. With the magnetic nanoparticle-polymer composites attached to every single node (Figure 5(a)), we designed the tubular model to contract when a magnetic field is applied (Figure 5(b)) and go back to its initial form when the magnetic field is removed (Figure 5(c)).

Before designing the tubular model, we first fabricated 2d planar anti-trichiral honeycomb unit cells with aligned magnetic nanoparticle-polymer composites to confirm the deformation under magnetic fields. Composites are arranged in the vacant nodes at $\theta_{xy} = \pm 45^\circ$.

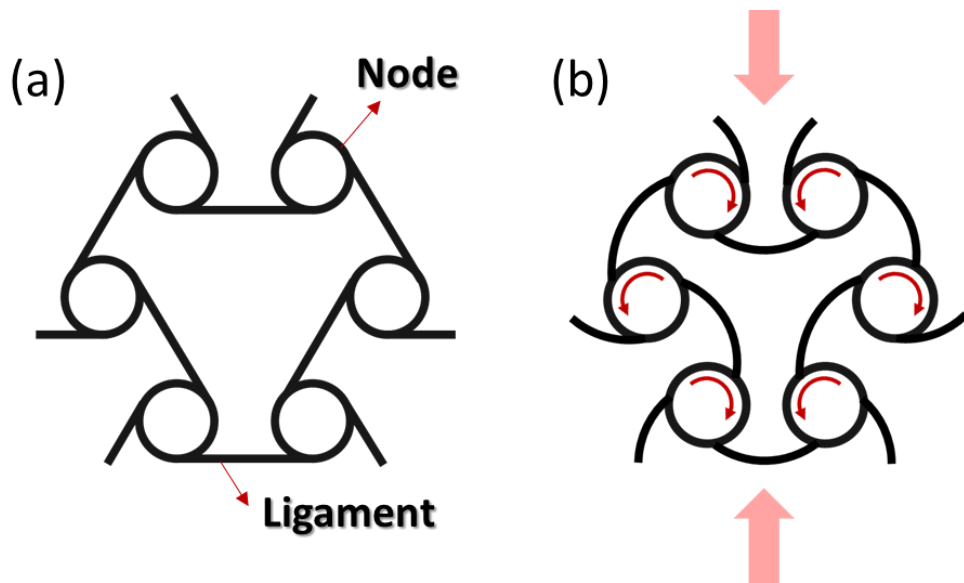


Figure 3 (a) Unit cell of anti-trichiral honeycomb structure (b) compressed state.

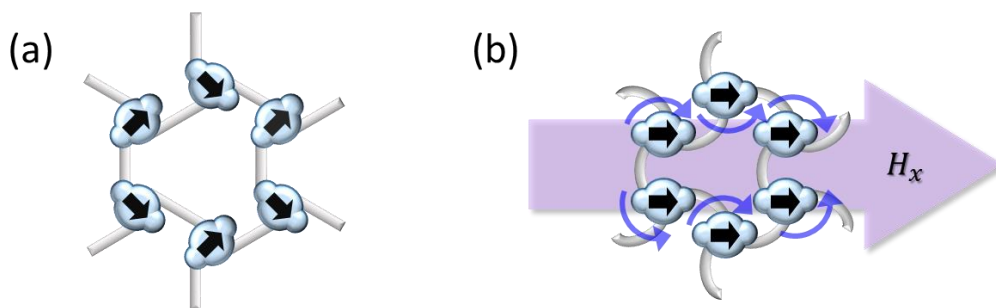


Figure 4 Illustration of an anti-trichiral honeycomb unit cell with magnetic nanoparticle-polymer composites, actuated under magnetic fields.

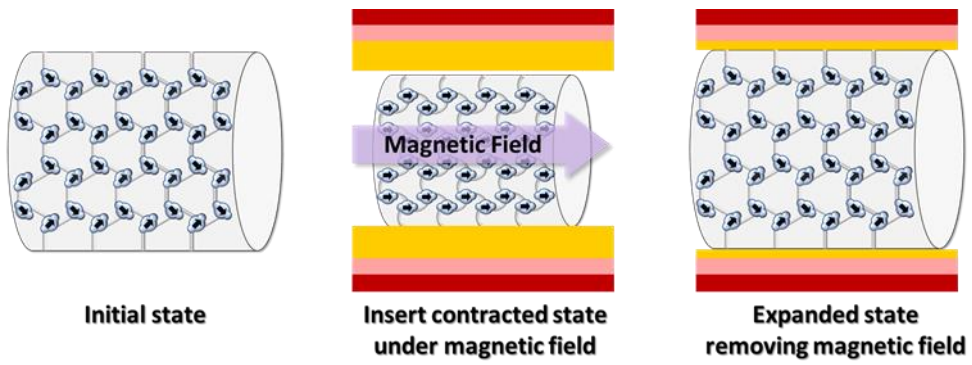


Figure 5 Concept of a magnetically actuated stent

3.2. Modeling

The magnetic actuation of the planar and tubular stent follows the same rotation mechanism but differ in terms of the connection between the ends which affects the movement of adjacent components. The actuation is induced by the magnetic anisotropy of the magnetic nanoparticle chains within each composite when the magnetic field is applied. We use the theoretical calculation of $2d$ in order to predict the magnetic nanoparticle–polymer composite rotation, which will induce the contraction of the whole structure.

There are a few assumptions: sphere–shaped single domain particles, assembled parallel to the applied magnetic field, and only dipolar interaction are considered, where interaction between adjacent chains are neglected. Calculation was done on a single composite, due to the independent movements of the composites.

Here, the magnetic actuation depends on the magnetic torque between dipolar interaction energy and Zeeman energy, and the mechanical torque induced by the bending of ligaments. The equilibrium of the torque will result in the magnetic actuation.

As illustrated in Figure 6, when chains are placed at an angle of θ with the magnetic field, the MNP dipoles are rotated by a moment angle α . The magnetic dipolar energy of one neighboring atom can be

expressed by [22, 23]:

$$E_{12} = \frac{\mu_0}{4\pi} \left(\frac{m_1 m_2}{d^3} \right), \vec{m}_1 \cdot \vec{m}_2 - 3(\vec{m}_1 \cdot \vec{d})(\vec{m}_2 \cdot \vec{d}) \quad (1)$$

\vec{m}_1 and \vec{m}_2 are the moment of the MNPs, and \vec{d} is the center-to-center interparticle separation (unit vector), and $\mu_0 = 4\pi \times 10^{-7} \text{kgms}^{-2}\text{A}^{-2}$ is the magnetic constant.

For a chain of identical MNPs,

$$\vec{m}_1 = \vec{m}_2 = \vec{m} \dots$$

$$E_{12} = \frac{\mu_0}{4\pi} \left(\frac{m^2}{d^3} \right) (1 - \cos^2 \alpha)$$

For infinitely long chains with 2, 3, 4... neighboring MNPs on each side, and by referring the Apéry's theorem,

$$E_{1^\infty} = 2E_{12} \sum_1^\infty \frac{1}{n^3}$$

$$\sum_1^\infty \frac{1}{n^3} = 1.202 \dots$$

For N MNPs,

$$E = \frac{0.6\mu_0 N}{\pi} \left(\frac{m^2}{d^3} \right) (1 - \cos^2 \alpha)$$

The magnetic torque, T_m , acting on the moments is therefore:

$$T_m = \frac{dE_m}{d\alpha} = -\frac{1.8\mu_0 N}{\pi} \left(\frac{m^2}{d^3} \right) (\sin 2\alpha)$$

The Zeeman Energy is

$$E_z = -\vec{m} \cdot \vec{B}$$

For N MNPs

$$\begin{aligned} E_z &= -N\vec{m} \cdot \vec{B} \\ &= -Nm\mu_0 H \cos(\theta - \alpha) \end{aligned}$$

The magnetic torque T_z , to rotate counterclockwise towards the external magnetic field is

$$T_z = -\frac{dE_z}{d\alpha} = Nm\mu_0 H \sin(\theta - \alpha)$$

The equilibrium of the magnetic moments (Figure 7) is

$$\begin{aligned} T_z + T_m &= 0 \\ Nm\mu_0 H \sin(\theta - \alpha) - \frac{1.8\mu_0 N}{\pi} \left(\frac{m^2}{d^3} \right) (\sin 2\alpha) &= 0 \\ H &= \frac{1.8m}{\pi d^3} \frac{\sin 2\alpha}{\sin(\theta - \alpha)} \end{aligned}$$

The derived equations above assume that the MNPs assemble into single chains of one MNP wide, along the long axis. However, in reality, the chains are assembled in long straight clusters of multiple MNPs wide. This affects the dipolar interaction of the MNPs along the short axis, and the followings are equations which the effective moment is considered:

$$H = 0.3\gamma M_s \frac{\sin 2\alpha}{\sin(\theta - \alpha)}$$

Γ is the disorder parameter and M_s is the saturation magnetization.

Similar to the previous work in [16], there are bending torques

of the ligaments, T_s , as the composites rotate.

$$T_s = -E_s \frac{a^3 b}{6L_{eff}} (\beta - \theta)$$

E_s is the elastic modulus of the elastomer, β [radians] is the maximum angle that the chain makes with the applied magnetic field Bx , and a , b , l are the thickness, width and length of the ligament, respectively.

$$*L_{eff} = L_y - 2\sqrt{2ra - a^2}$$

L_{eff} represents the effective ligament length, as illustrated in Figure 11(a).

By considering three ligaments for the composite, the equilibrium of the mechanical torque (Figure 8) will be the following:

$$T_c - 3T_s = 0$$

$$\sin 2\alpha = \frac{\pi d^3 a^3 b}{3.6\mu_0 N m^2 L_{eff}} E_s \left(\frac{\pi}{4} - \theta \right)$$

$$\sin 2\alpha = \frac{\rho a^3 b}{0.6\mu_0 f w \gamma^2 M_s^2 L_{eff}} E_s \left(\frac{\pi}{4} - \theta \right)$$

Through analysis of the torque and its equilibrium, the mathematical model of the 2D actuation can be accomplished. Figure 9 is the theoretical calculation of chain angle rotation according to magnetic field.

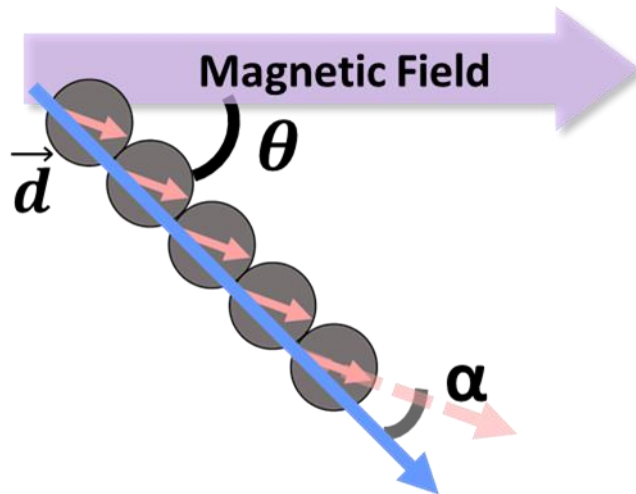


Figure 6 Illustration of Zeeman Energy

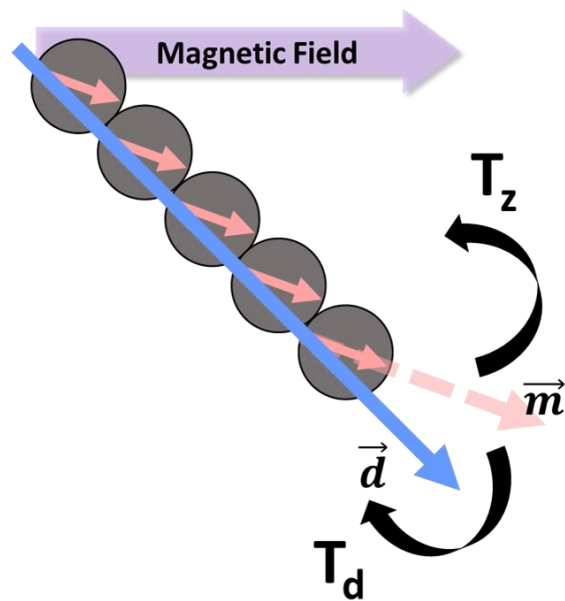


Figure 7 Magnetic moments of dipolar interaction energy and Zeeman energy

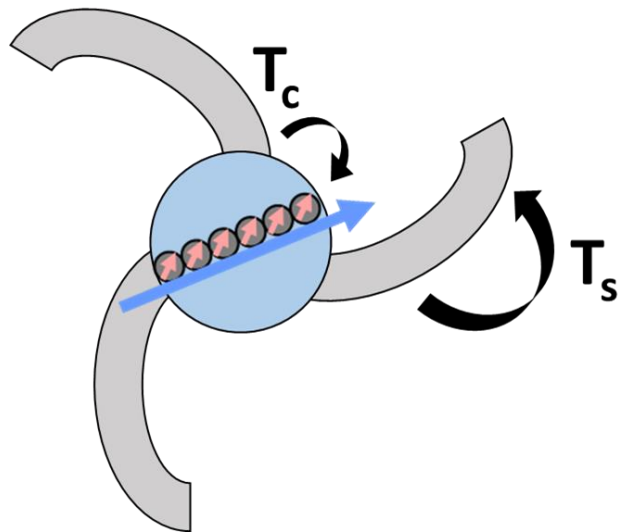


Figure 8 Torque of magnetic moment and elastic energy

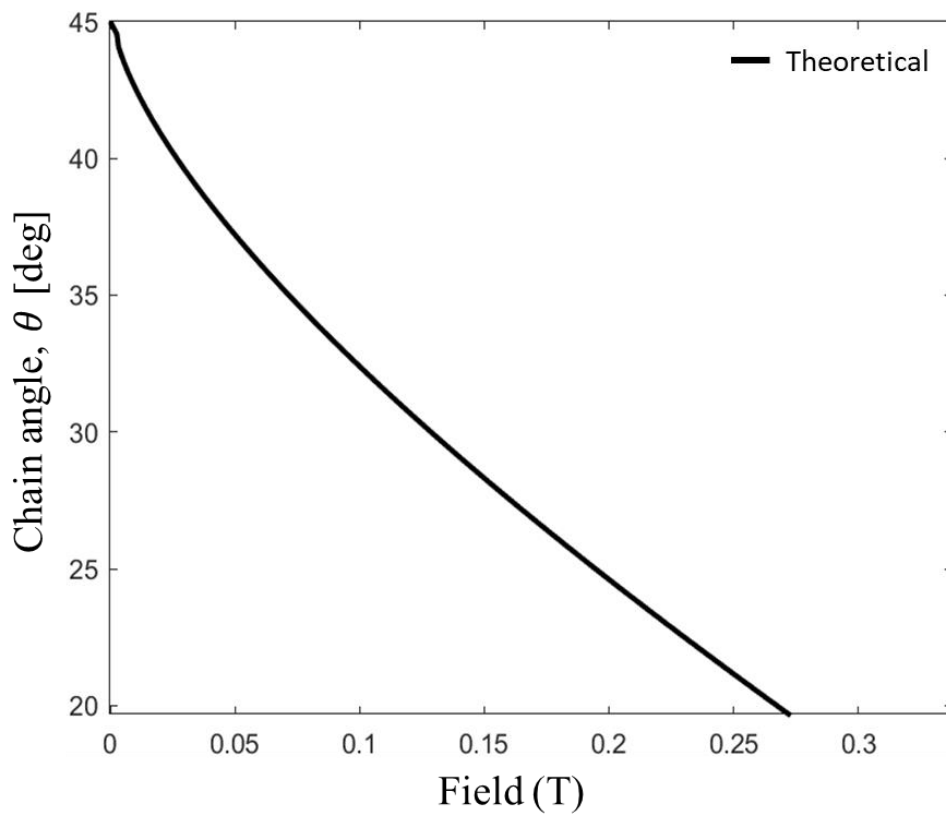


Figure 9 Theoretical calculation of chain angle rotation according to magnetic field

Chapter 4. Sample Fabrication

This chapter describes the fabrication method of the 3D printed anti-trichiral tubular structure with magnetic nanoparticles-polymer composite. Schematic illustrations of the 3D structures, chain directions, and the corresponding actuated profiles are shown. A detailed fabrication method, including the dimensions and the materials used, can be found in this chapter.

4.1. Fabrication Method

The fabrication method of the magnetic stent involves a three-step process. The first step is the 3D printing of the planar and tubular anti-trichiral honeycomb structure. The second step is the functionalization of the magnetic composites by aligning the MNPs into chains. The final step is the assembly of composites by attaching them onto the 3D printed structures.

4.1.1 3D Printing of anti-trichiral honeycomb structure

A commercial SLA 3D printer (Formlabs Inc., Form2 printer) equipped with a 405 nm laser was utilized for printing the anti-trichiral tubular structure (Figure 10). The printer allows fabrication of objects with a resolution of 300 mm and a layer thickness of 25, 50, 100 or 200 mm. The templates used to print the structures were designed with Autodesk Inventor professional and exported as a stereolithography file (.stl) into the 3D printer software (Preform Software). The photocurable flexible resin material (Formlabs, elastic 50A) was set up as elastic and the layer thickness was 0.1mm.

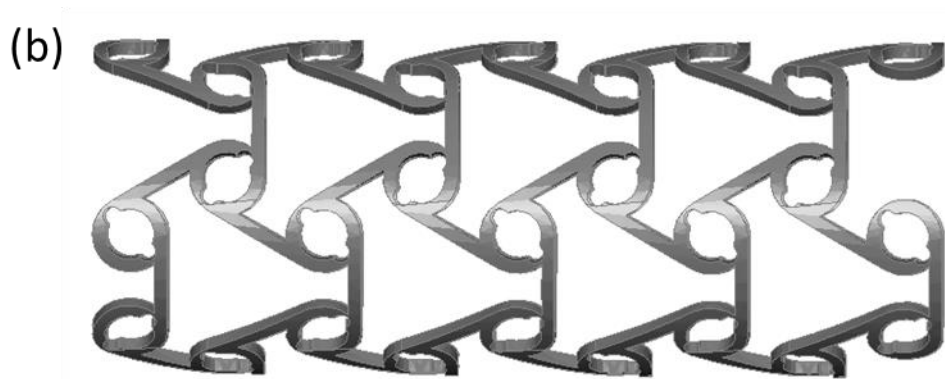
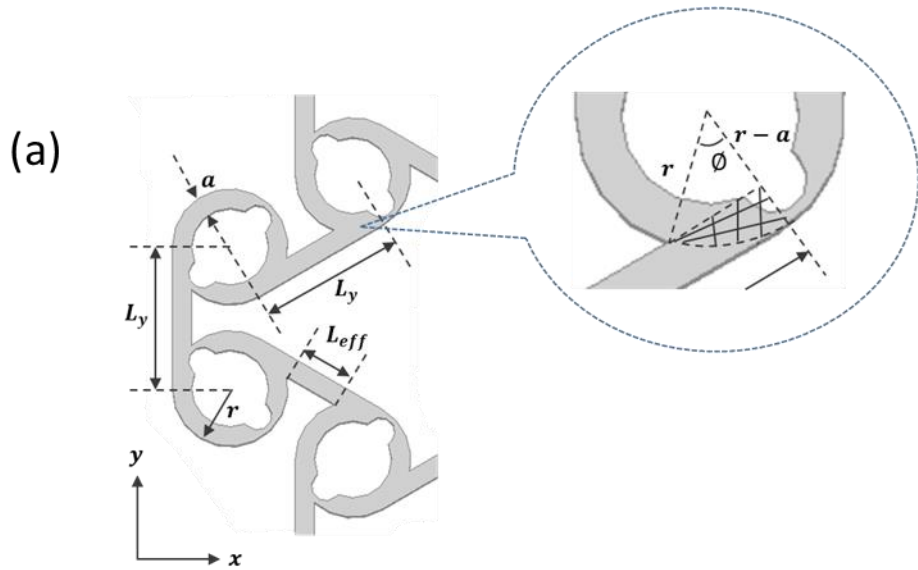


Figure 10 a) Unit cell and (b) tubular design of anti-trichiral honeycomb structure

4.1.2 Alignment Mold

A 3D printed mold is used for the fabrication of magnetic nanoparticle–polymer composites, where they are used for the alignment of the MNPs in the second step process. The mold was designed on a 3D CAD software (Inventor Professional, Autodesk) and printed by a stereolithography (SLA) 3D printer (Kings 1700, KINGS3D). Fabricating molds using a SLA printer produce a high quality and high resolution product, good for manufacturing complex and precise composites.

The alignment mold is shown in Figure 11, which consists of 2 layers, top and bottom to make composites considering the curvature of the tubular structure. The dimensions of the composites used in this study are summarized in Table 1.

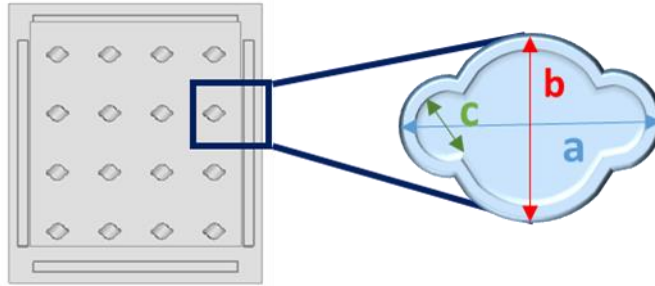


Figure 11 Alignment mold for magnetic nanoparticle-polymer composites.

Table 1 Dimensions of the alignment mold

Parameter	Length (mm)
a	2.75
b	2
c	0.75
depth	0.5

4.1.3 Material Preparation

For the stent structure, a photosensitive resin was prepared. An elastic engineering resin (Formlabs, Elastic 50A) was used for the SLA 3D printing.

Silicone elastomer (Xinuslab, SH2115) was prepared in order to make magnetic nanoparticle–polymer composites. Parts A and B were mixed thoroughly in a 1:1 ratio, and 35wt% of Fe_3O_4 iron oxide nanoparticles (Sigma–Aldrich, 637106) with an average size of 50–100 nm were added and mixed. The elastomer–nanoparticle mixture was then immediately poured into the assembly mold and placed in a magnetic field to make chains of magnetic nanoparticles in the field direction.

4.1.4 Alignment

The direction of which the magnetic nanoparticle chains are to be aligned is simply determined by the morphology of the actuated shape with respect to the direction of the magnetic field, H_x , which is the direction of the external uniform magnetic field used to align and actuate the magnetic stent. The alignment is performed by placing the alignment mold consisting of the uncured magnetic–nanoparticle elastomer mixture in a uniform magnetic field of 40 mT that is generated from the electromagnet (Figure 12). Before the elastomer matrix is cured, the magnetic nanoparticles in the mixture move and self–assemble into chains in the direction of the applied magnetic field, such that when the elastomer matrix is cured, the chains are permanently embedded within the matrix. The curing time of the composite is approximately 4–5 hours, as the curing time of the Si elastomer is 4–5 hours.

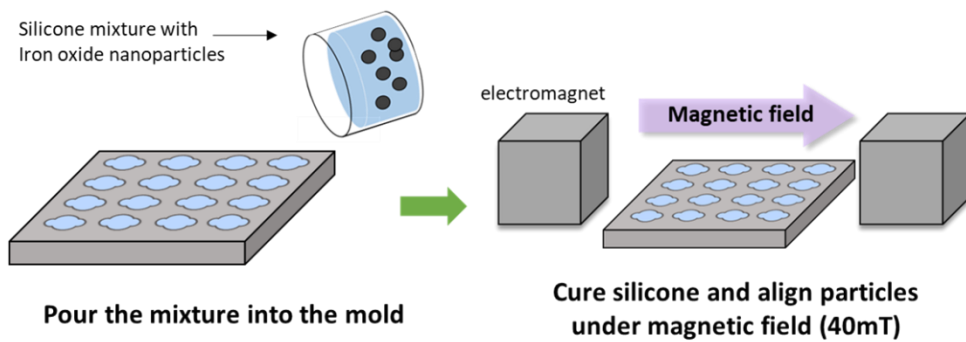


Figure 12 Illustration of the fabrication process of magnetic nanoparticle-polymer composites

4.1.5 Assembly

The final step of the fabrication process is the assembly of the aligned composites to the printed stent structure. The stent structure is printed with many supporting structures that prevent overhanging or bridge structure when printing. The supporting structures are removed with a small nipper carefully.

The aligned composites can be removed from the alignment mold with tweezers and attached onto the structure in the appropriate place shown in Figure 13. The composites can be attached by applying a silicone adhesive (Smooth-on, Sil-Poxy) on the borders of the node, and dried for 24 hrs.

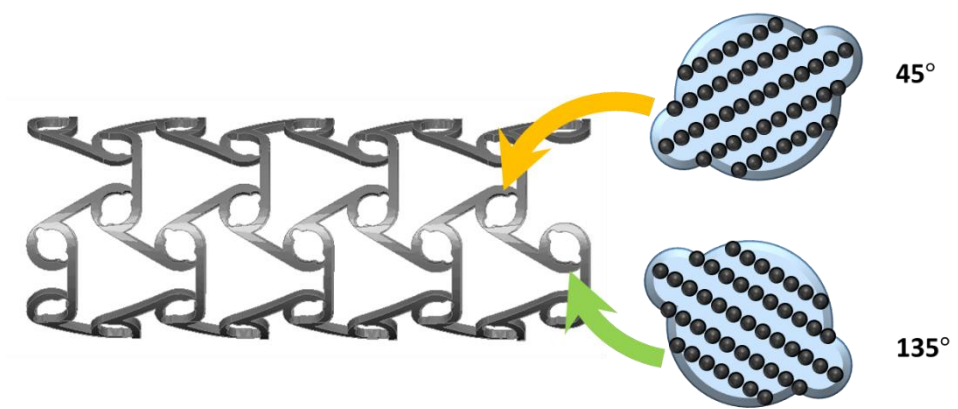


Figure 13 Attachment of the magnetic nanoparticle-polymer composites

Chapter 5. Results

This chapter shows all the 2D modeling results, experimental results, and 3D experimental results. The experimental results are compared with the 2D modeling results. The VSM and optical microscopy (OM) results are also included.

5.1. Magnetic Properties and Characterization

In order to confirm the magnetic chain alignment of the magnetic nanoparticle–polymer composite, parallel and perpendicular samples were prepared. The samples were characterized by an optical microscope and the vibrating sample magnetometer (VSM).

5.1.1 Optical Microscopy

Figure 14(a) shows a schematic of the aligned composite. An optical microscopic image was taken to confirm the alignment of the magnetic nanoparticle chains induced by the magnetic field. In Figure 14(b), the dark horizontal lines confirm the alignment of the chains embedded in the elastomer composite.

5.1.2 Vibrating sample magnetometer

To verify the magnetic anisotropy due to chain formations, the vibrating sample magnetometer (Lake-shore, VSM-7410) was used. Hysteresis loops of samples of the chain long axis parallel and perpendicular to the magnetic field direction were measured. Figure 14(c) shows the different hysteresis loops between the two samples. The parallel sample has the higher magnetization, since the magnetic nanoparticle chains are aligned in the magnetic field direction. This means an energetically stable state. The perpendicular sample has the lower magnetization, due to the chain alignment perpendicular to the magnetic field direction. These results confirm the magnetic anisotropy of the composite and the direction dependent properties, allowing the magnetic actuation.

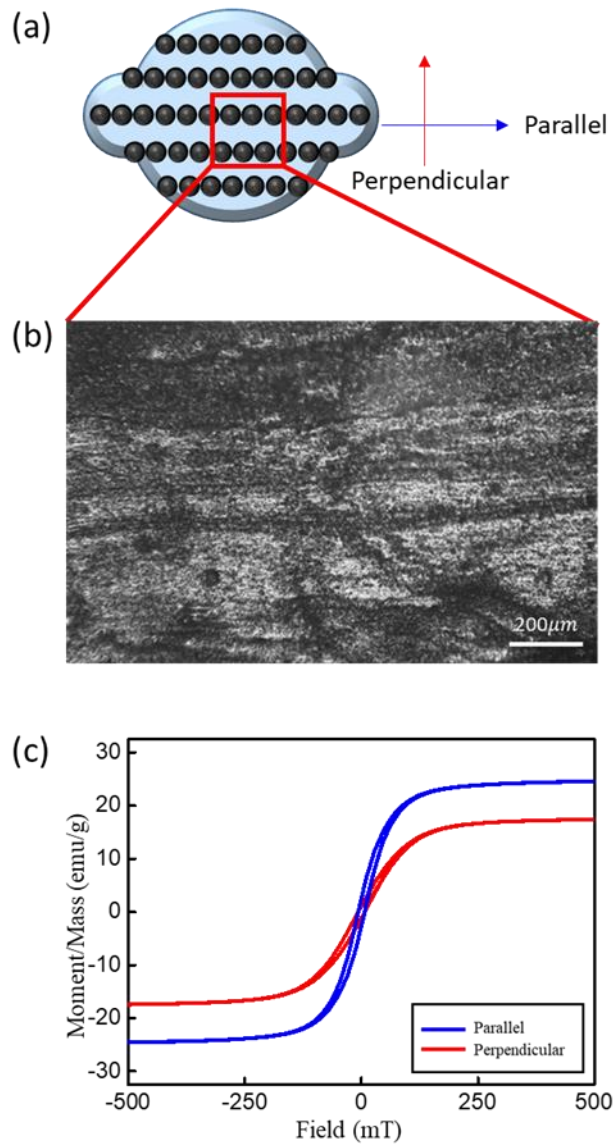


Figure 14 (a) Schematic of the magnetic nanoparticle-polymer composite. Arrows indicate the parallel and perpendicular direction. (b) Optical microscopic image and (c) hysteresis curves measured by VSM.

5.2. Magnetic actuation of 2D anti-trichiral honeycomb structure

The 2D anti-trichiral prototype was placed between the poles of the electromagnet. Under various magnetic fields up to 250 mT, the magnetic composites of the fabricated 2D anti-trichiral prototype rotates to arrange the chains parallel to the field direction. Rotation is accompanied by the bending of ligaments. As shown in Figure 15(a), the red box indicates the contraction under magnetic fields, confirming a negative Poisson's ratio. Figure 15(b) shows the chain rotation angle according to the magnetic fields. The chain rotation has the highest value at 165mT.

The experimental values are plotted on the theoretical modeling results in Figure 16. In the theoretical results, the variation of the chain rotation angle consistently increases as the magnetic field increases. However, in the experimental results, rotation was done only until 165mT. The deviations may be a result of energy loss due to the fabrication method, where the magnetic nanoparticle-polymer composites are attached by an adhesive. It was confirmed that even under a low magnetic field, actuation of the anti-trichiral honeycomb structure can be conducted.

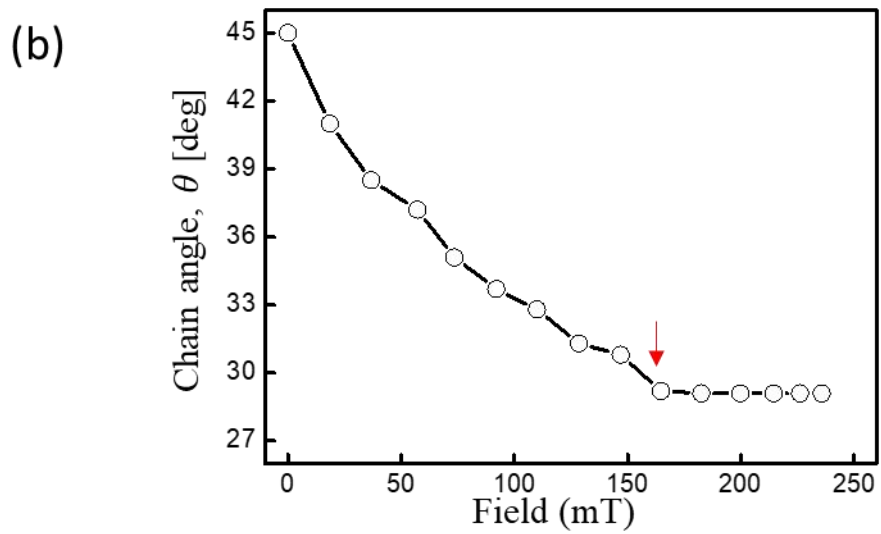
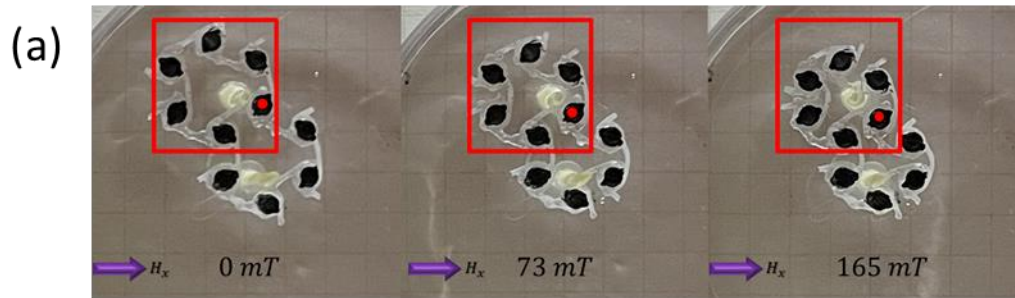


Figure 15 (a) Images of the 2D prototype under various magnetic fields. (b) Chain rotation angle under various magnetic fields.

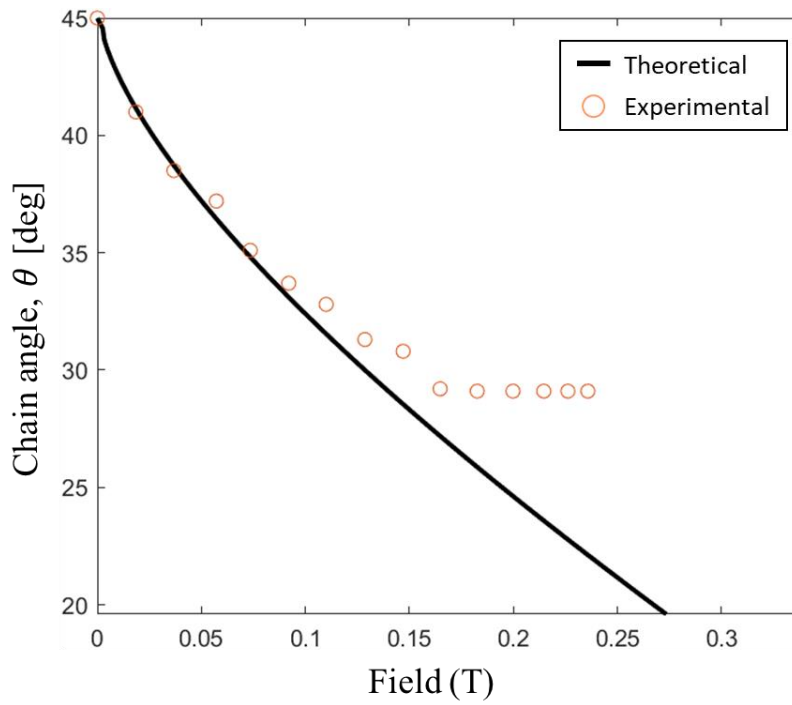


Figure 16 Comparison of the theoretical modeling and experimental values.

5.3. Optimization of parameters for stent design

Based on the comparison of the theoretical and experimental results in chapter 5.2., more work was done in order to find the optimal geometrical parameters. Five different stent prototypes were used for investigation. Figure 17 illustrates the major parameters, and Table 2 provides the values of each parameter. Stent No. A, B, C were set to have different stent thickness values (0.75 mm, 0.625 mm, 0.5 mm), and C, D, E were set to have different ligament length (3.64 mm, 4 mm, 4.5 mm).

Prior to the experiments, theoretical calculation was done in order to predict the tendency of the actuation. Figure 18 are the results with (a) different stent thickness, and with (b) different ligament length. According to the results, rotation variation was shown to be larger with thinner thickness and longer ligaments.

Experiment results on stent thickness showed similar rotation chain angles to each other in Figure 19(a), while over 100mT, the tendency was same as the prediction. For ligament length in Figure 19(b), over 100mT, rotation variation was higher for the sample with longer ligament lengths.

Figure 20 shows the experimental results plotted on the

theoretical results. Due to the random tendency between the samples with varying stent thickness, the theoretical values seemed to not match the results. The values matched well for the samples with varying ligament length under 200mT. It was confirmed that ligament length is the significant parameter compared to stent thickness.

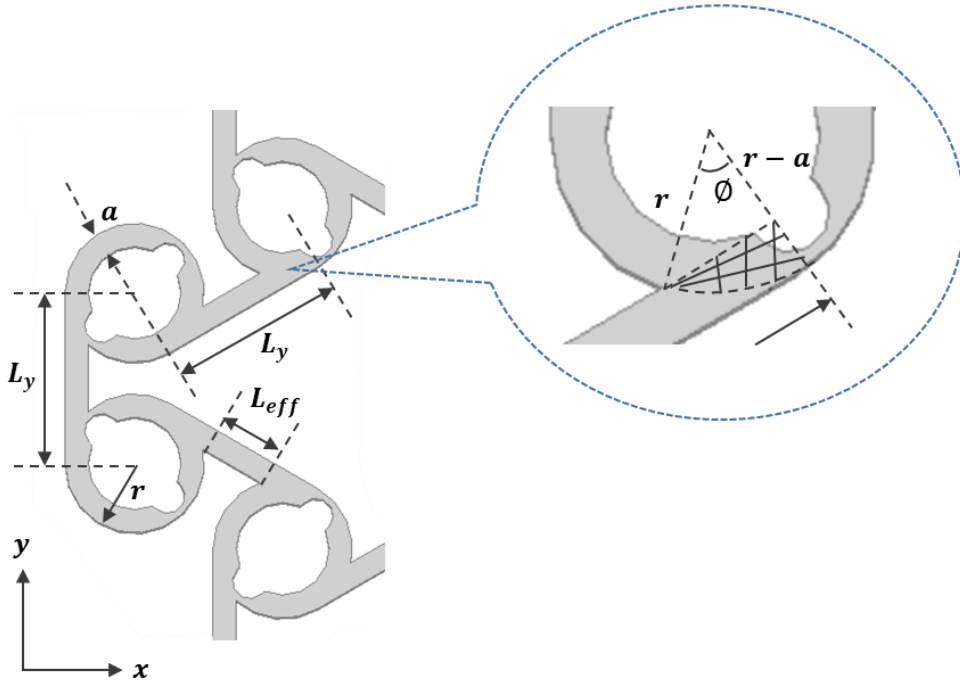


Figure 17 Illustration of major parameters of anti-trichiral honeycomb structure.

Table 2 Table 2. Values of the stent parameters.

Stent No.	$D_{inner}(\text{mm})$	$b(\text{mm})$	$L_y(\text{mm})$
A	10	0.75	3.72
B	10	0.625	3.68
C	10	0.5	3.64
D	11	0.5	4
E	12.5	0.5	4.5

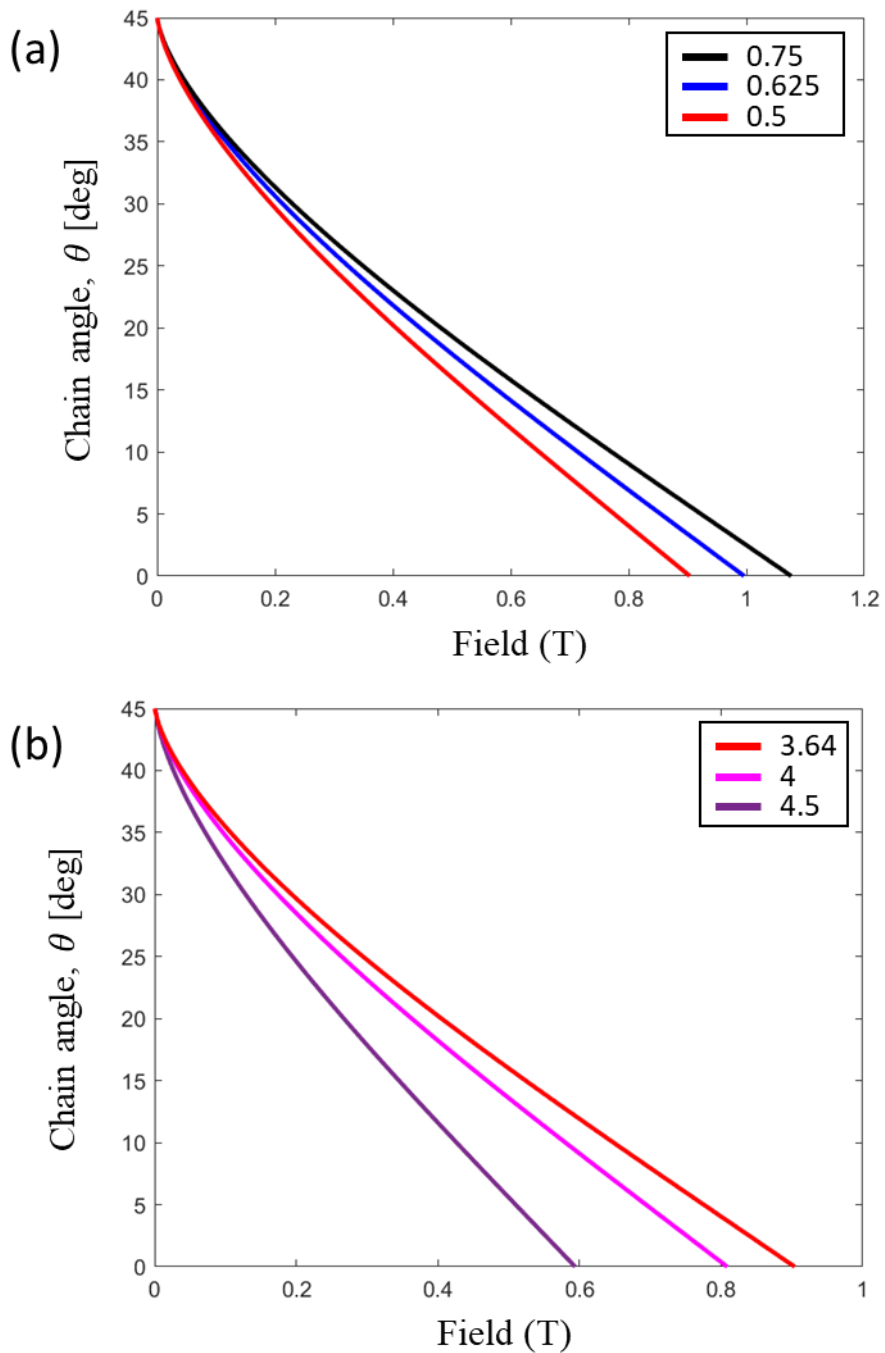


Figure 18 Theoretical calculation results with (a) with different stent thickness, and (b) different ligament length

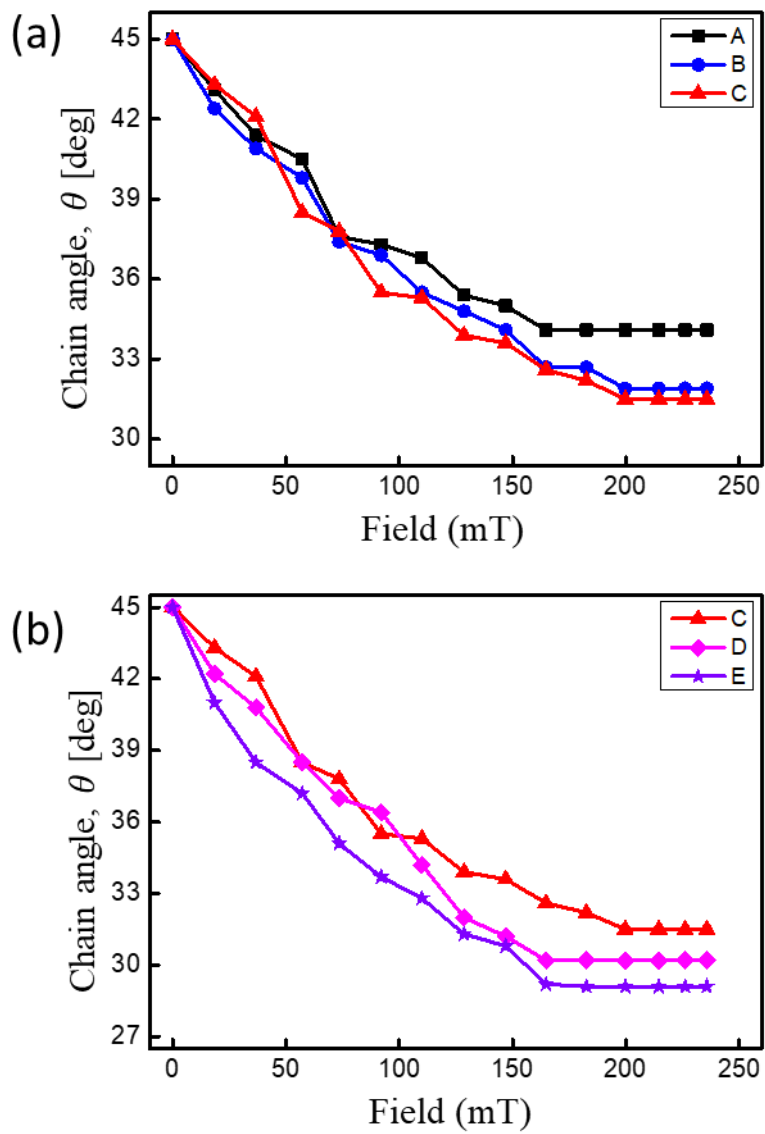


Figure 19 Experimental results of stents (a) with different stent thickness, and (b) different ligament length

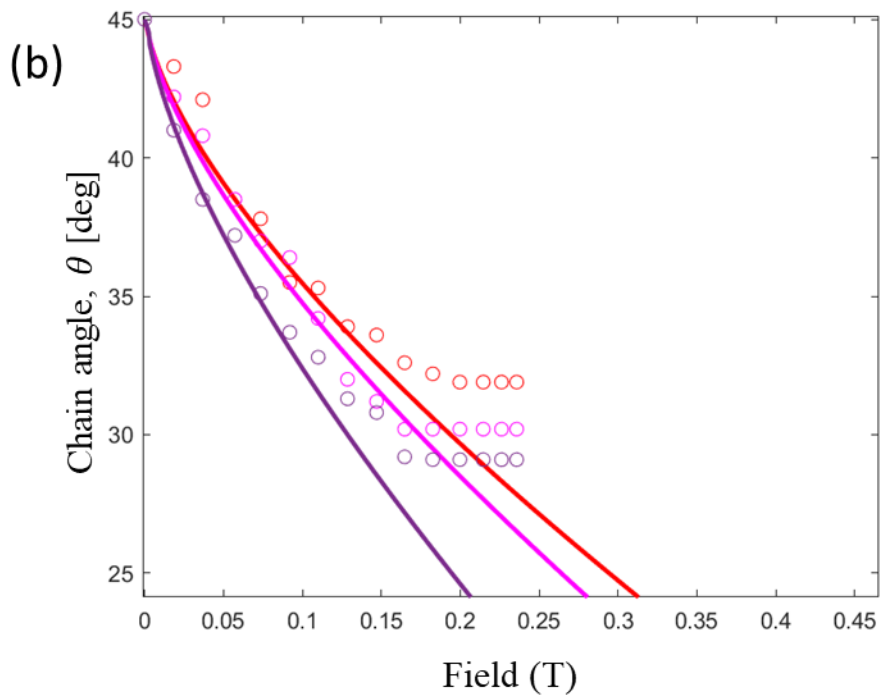
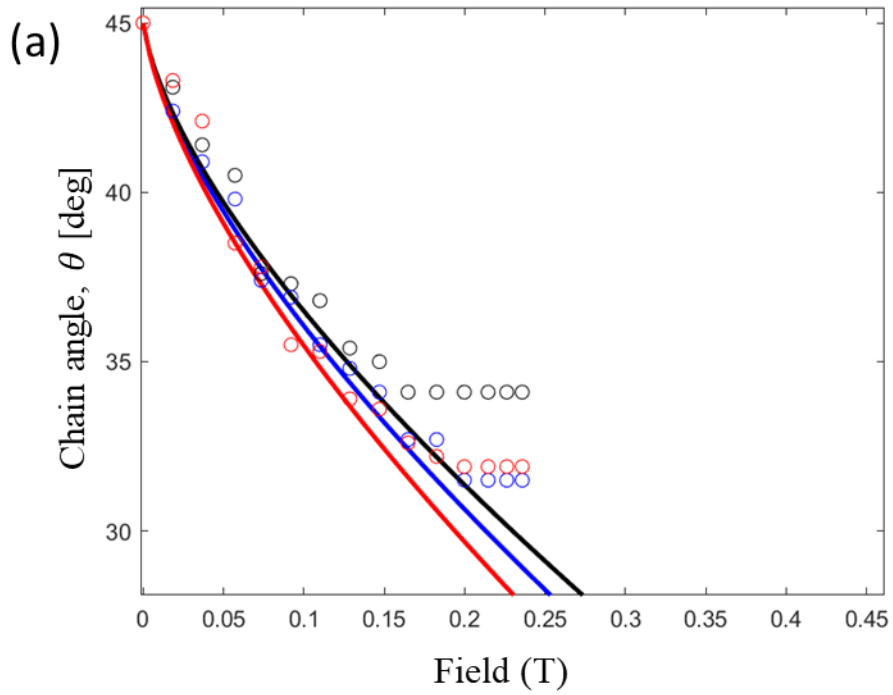


Figure 20 Comparison of theoretical and experimental results of stents (a) with different stent thickness, and (b) different ligament length.

5.4. Optimization of 3D stent

Based on the 2D parameter optimization results, 3D prototypes with the same value (Table 2) were also fabricated, in order to compare and analyze the chain angle rotation and contraction rates of the length in the axis direction and diameter of the tubular structure. Experiments on 3D prototypes with the same variation of stent thickness and ligament length were conducted.

5.4.1 Contraction according to stent thickness

Figure 21 shows the chain rotation results of the 3D prototypes with different stent thicknesses (0.75 mm, 0.625 mm, 0.5 mm). With varying stent thickness values, the thickest sample showed the bigger rotation value, while the rotation value tendency not matched with the 2D results.

The contraction rates of the length in the axis direction and diameter were evaluated in Figure 22. Figure 22(a) indicates the length and diameter of the tubular prototype. Figure 22(b), which is the length contraction rate, contraction was confirmed in all samples, where contraction stops around 200mT. Figure 22(c) is the diameter

contraction rate; thinner samples show better contraction behavior, where the sample with 0.5 mm thickness shows the highest contraction rate.

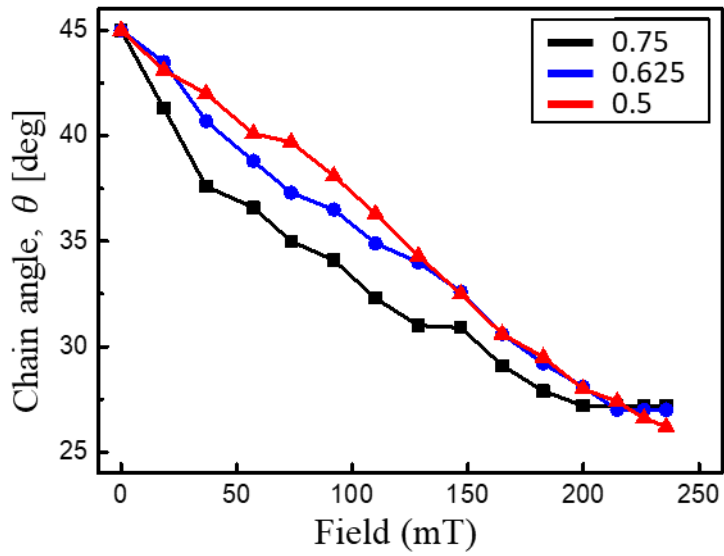


Figure 21 Experimental results for 3D stent chain angle rotation with different stent thickness

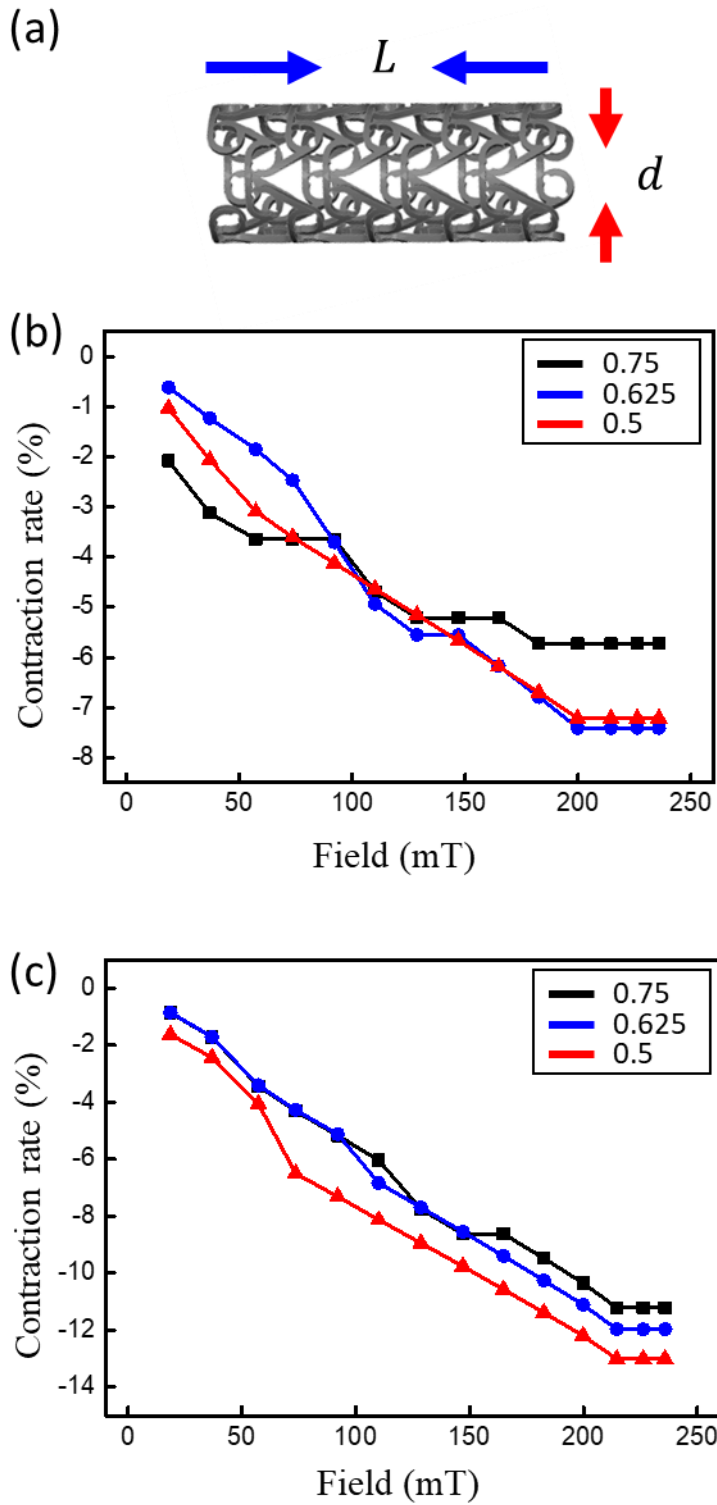


Figure 22 Contraction rate of samples with different stent thickness, (a) length in the axis direction and (b) diameter.

5.4.2 Contraction according to ligament length

Figure 23 shows the chain rotation values of samples with different ligament length, where longer samples showed the better variation. As well as the 2D results, the 3D results also confirmed that ligament length is the more significant factor for stent actuation.

In Figure 24(a), the length contraction stopped around 180mT, while in Figure 24(b) diameter contraction stopped over 200mT. Under low magnetic fields, the optimal ligament length is 4 mm. Also, 4 mm was confirmed to show the best contraction behavior in both length and diameter values.

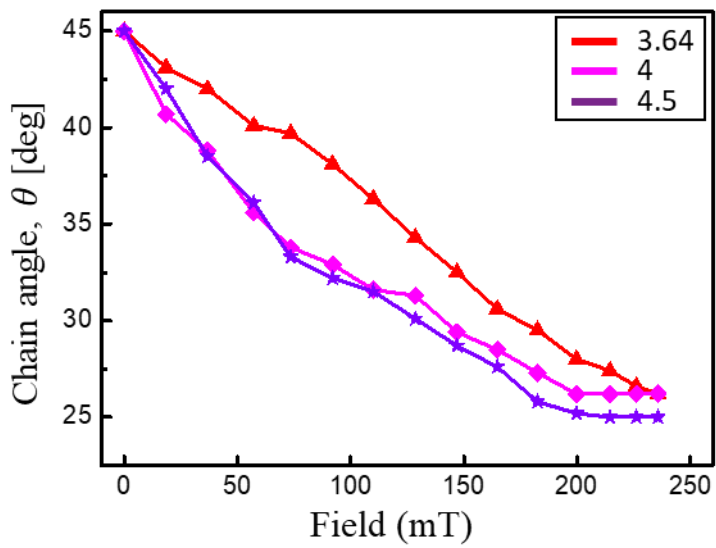


Figure 23 Experimental results for 3D stent chain angle rotation with different ligament length.

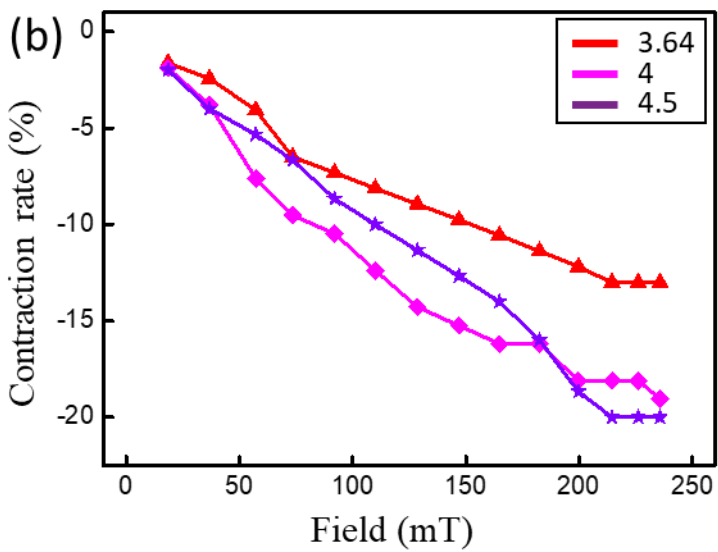
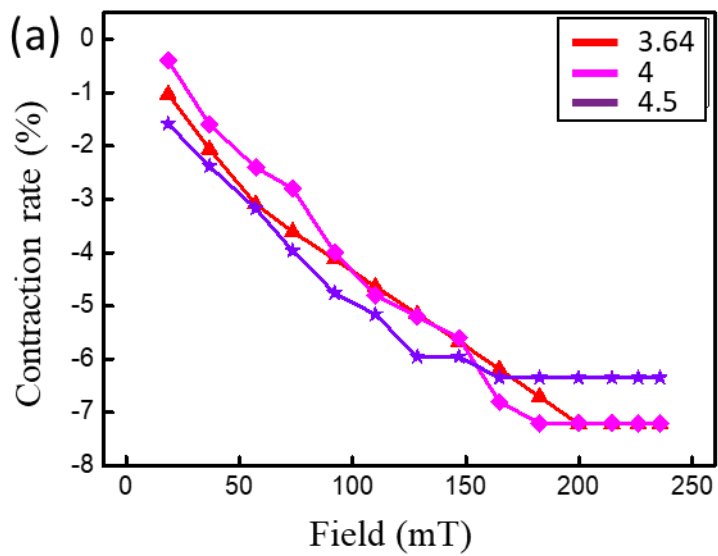


Figure 24 Contraction rate of samples with different ligament lengths (a) length in the axis direction and (b) diameter.

5.4.3 Optimized 3D stent prototype

Based on the optimal values, we eventually fabricated a stent with optimized thickness and ligament length values. The magnetic actuation of the optimized stent prototype was measured under various magnetic fields. Figure 25(a) shows the contraction behavior of the prototype under 0 mT, 110 mT, and 200 mT. Chain rotation of the magnetic–nanoparticle polymer composites were confirmed to increase under higher magnetic fields, where the maximum was at 200 mT (Figure 25(b)). Figure 26(a) shows the contraction rate of the length in the axis direction, which has the maximum contraction rate at 180 mT. The contraction rate of the diameter shows the maximum contraction rate at 200 mT, in Figure 26(b).

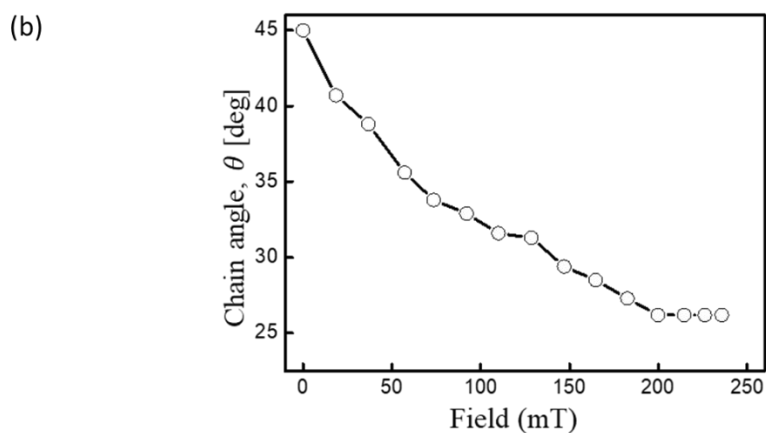
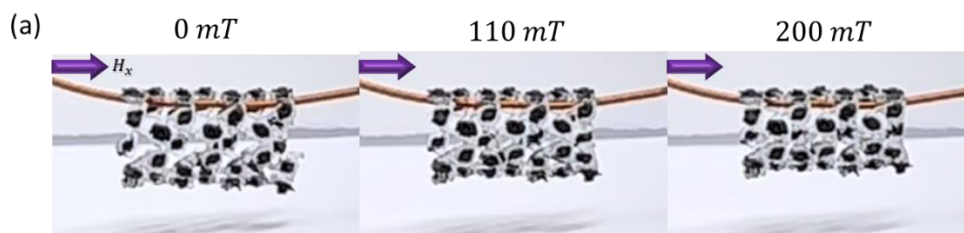


Figure 25 (a) Images of the contracting anti-trichiral stent composed of magnetic nanoparticle-polymer composites and (b) chain rotation angle under various magnetic fields.

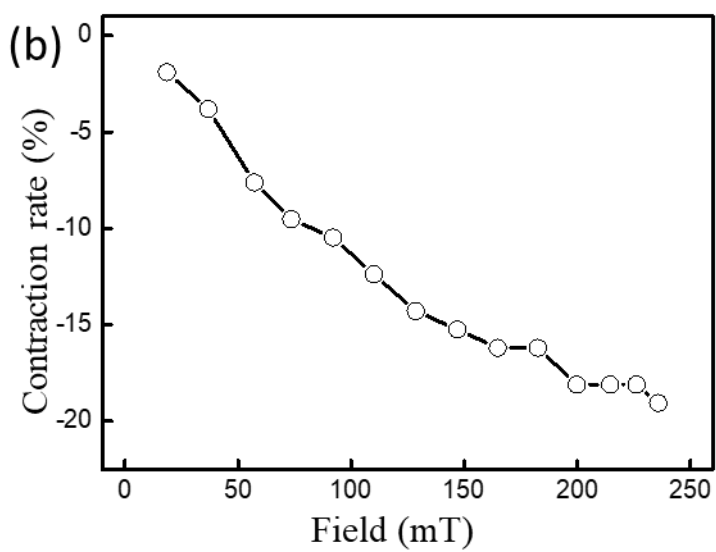
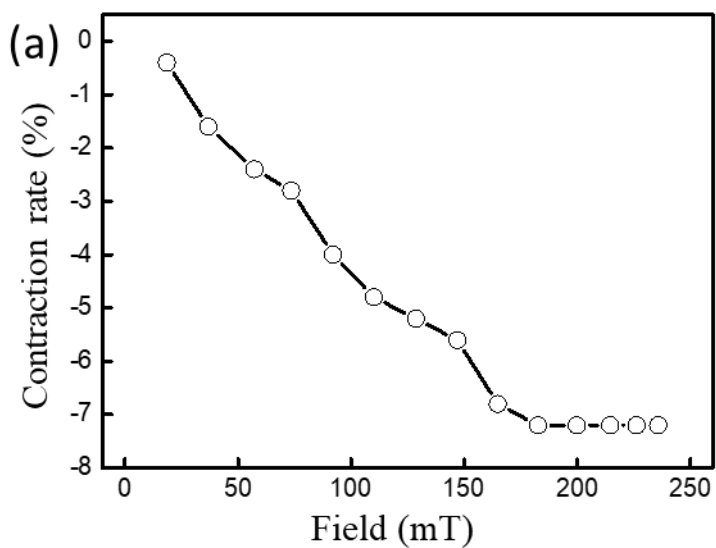


Figure 26 Contraction rate of (a) length in the axis direction and (b) diameter.

Chapter 6. Conclusion

In this study a 3D printed anti-trichiral stent with aligned magnetic nanoparticle-polymer composites was fabricated. Due to the magnetic anisotropy of the magnetic nanoparticles embedded in the composites, chain rotation was confirmed under various magnetic fields, resulting in the actuation of the structure.

Theoretical modeling was done to predict the chain rotation behavior of the composites. Rotation properties of 2D prototypes were compared with the theoretical results, which matched under low magnetic field strengths. Based on the 2D results, various types of stents were fabricated for optimization of the geometrical parameters of the auxetic chiral stent composed of magnetic nanoparticle-polymer composites. Maximum contraction behavior was confirmed from the optimized prototype.

This study provided a conceptual demonstration of the magnetically expandable auxetic polymer stent. The results may show the possibility of applications of a novel self-expandable stent method.

References

1. Schmidt, T. and J.D. Abbott, *Coronary Stents: History, Design, and Construction*. J Clin Med, 2018. **7**(6).
2. Stefanini, G.G. and D.R. Holmes, *Drug-Eluting Coronary-Artery Stents*. New England Journal of Medicine, 2013. **368**(3): p. 254–265.
3. Kereiakes, D.J., et al., *Bioresorbable Vascular Scaffolds for Coronary Revascularization*. Circulation, 2016. **134**(2): p. 168–182.
4. Xue, L., S. Dai, and Z. Li, *Biodegradable shape-memory block copolymers for fast self-expandable stents*. Biomaterials, 2010. **31**(32): p. 8132–8140.
5. Hu, W., et al., *Small-scale soft-bodied robot with multimodal locomotion*. Nature, 2018. **554**(7690): p. 81–85.
6. Zhang, X., et al., *Optically- and Thermally-Responsive Programmable Materials Based on Carbon Nanotube-Hydrogel Polymer Composites*. Nano Letters, 2011. **11**(8): p. 3239–3244.
7. Li, L., J.M. Scheiger, and P.A. Levkin, *Design and Applications of Photoresponsive Hydrogels*. Advanced Materials, 2019. **31**(26): p. 1807333.
8. Deng, H., et al., *Bioinspired multi-responsive soft actuators controlled by laser tailored graphene structures*. Journal of Materials Chemistry B, 2018. **6**(34): p. 5415–5423.

9. Toncheva, A., et al., *Bilayer solvent and vapor-triggered actuators made of cross-linked polymer architectures via Diels–Alder pathways*. *Journal of Materials Chemistry B*, 2017. **5**(28): p. 5556–5563.
10. Schmauch, M.M., et al., *Chained Iron Microparticles for Directionally Controlled Actuation of Soft Robots*. *ACS Applied Materials & Interfaces*, 2017. **9**(13): p. 11895–11901.
11. Kim, Y., et al., *Printing ferromagnetic domains for untethered fast-transforming soft materials*. *Nature*, 2018. **558**(7709): p. 274–279.
12. Xu, T., et al., *Millimeter-scale flexible robots with programmable three-dimensional magnetization and motions*. *Sci Robot*, 2019. **4**(29).
13. Huang, H.-W., et al., *Adaptive locomotion of artificial microswimmers*. *Science Advances*, 2019. **5**(1): p. eaau1532.
14. Cianchetti, M., et al., *Biomedical applications of soft robotics*. *Nature Reviews Materials*, 2018. **3**(6): p. 143–153.
15. Boczkowska, A. and S. Awietjan. *Microstructure and Properties of Magnetorheological Elastomers*. 2012.
16. Jiralerspong, T., et al., *Wireless Control of Two- and Three-Dimensional Actuations of Kirigami Patterns Composed of Magnetic-Particles-Polymer Composites*. *ACS Nano*, 2020. **14**(12): p. 17589–17596.
17. Ren, X., et al., *A simple auxetic tubular structure with tuneable mechanical properties*. *Smart Materials and Structures*, 2016. **25**.
18. Yang, L., et al., *Mechanical properties of 3D re-entrant honeycomb auxetic structures realized via additive manufacturing*. *International*

- Journal of Solids and Structures, 2015. **69-70**: p. 475-490.
19. Sangsefidi, A., et al., *An Abaqus plugin for evaluation of the Auxetic structure performance*. Engineering with Computers, 2021. **38**: p. 1-24.
 20. Alomarah, A., D. Ruan, and S. Masood, *Tensile properties of an auxetic structure with re-entrant and chiral features—a finite element study*. The International Journal of Advanced Manufacturing Technology, 2018. **99(9)**: p. 2425-2440.
 21. Mousanezhad, D., et al., *Elastic properties of chiral, anti-chiral, and hierarchical honeycombs: A simple energy-based approach*. Theoretical and Applied Mechanics Letters, 2016. **6(2)**: p. 81-96.
 22. Erb, R.M., et al., *Actuating Soft Matter with Magnetic Torque*. Advanced Functional Materials, 2016. **26(22)**: p. 3859-3880.
 23. Mishra, S.R., et al., *Selective and directional actuation of elastomer films using chained magnetic nanoparticles*. Nanoscale, 2016. **8(3)**: p. 1309-1313.

Abstract in Korean

심근경색, 협심증과 같은 관상 동맥 질환은 전 세계 주요 사망 원인 중 하나이다. 이를 치료하는 관상 동맥 중재술에는 대표적으로 풍선 혈관 성형술과 금속 스텐트(BMS)를 사용한 스텐트 시술이 이루어지고 있다. 하지만 BMS를 사용한 시술은 재협착, 혈전증, 심근경색 및 사망 위험의 증가라는 부작용들이 존재한다.

본 연구에서는 이러한 부작용 및 합병증을 극복하기 위해 자성나노입자-고분자 복합체로 구성되고 3차원 프린팅으로 제작된 어세틱 스텐트를 제시하였다. 자성나노입자에 자기장을 가하여 사슬 형태를 이루게 함으로써 자기 이방성을 설정하고, 스텐트 조작용을 위해 특정 위치에 부착하는 방식으로 제작하였다. 자기장 하에서 복합체의 움직임 분석을 위해 단일 복합체에 관한 모델링을 통해 자기장 세기에 따른 복합체의 회전에 관한 수식을 도출하였다. 250mT 이하의 자기장 하에서 진행된 실험 결과 160mT 이하의 영역에서 결과가 일치하는 양상을 보였다. 수치의 최적화를 통해 최종적으로 제작한 3차원 구조의 스텐트는 관의 축 방향을 따라 최대 250mT의 자기장 하에서 즉각적이고 반복적인 수축 및 확장 동작을 보이는 것을 확인하였다. 이는 기존의 풍선 혈관 성형술과 금속 스텐트의 한계를 극복하는 대안으로 자기장을 통한 원격조종을 통한 구동 방식을 제시한다.